

# Effects of Landau-Lifshitz-Gilbert damping on domain growth

Kazue Kudo

*Department of Computer Science, Ochanomizu University,  
2-1-1 Ohtsuka, Bunkyo-ku, Tokyo 112-8610, Japan*

(Dated: December 1, 2018)

Domain patterns are simulated by the Landau-Lifshitz-Gilbert equation with an easy-axis anisotropy, and they look similar to those of scalar fields. Even without the Gilbert damping, domains are formed, and they grow with time. Domain growth laws and small-scale structure are different between the cases with and without the damping. While domain walls become smooth because of the damping, they are rough in the no-damping case. However, large-scale domain patterns look similar in both cases. These long-scale and small-scale structures are characterized by different length scales.

PACS numbers: 89.75.Kd, 89.75.Da, 75.10.Hk

## I. INTRODUCTION

Coarsening dynamics is observed in a wide variety of systems. When a system is quenched from a disordered phase to an ordered phase, many small domains are formed, and they grow with time. For example, in the case of an Ising ferromagnet, up-spin and down-spin domains are formed, and the characteristic length of domain increases with time. The Ising spins can be interpreted as two different kinds of atoms in the case of a binary alloy. At the late stage of domain growth in these systems, characteristic length  $R(t)$  follows a power-law growth law,

$$R(t) \sim t^n, \quad (1)$$

where  $n$  is the growth exponent. The growth laws have been derived by several groups [1–4]:  $n = 1/2$  for non-conserved scalar fields, and  $n = 1/3$  for conserved scalar fields.

Similar coarsening dynamics and growth laws appear also in some vector fields with an easy-axis anisotropy. For example, in a two-dimensional ferromagnetic Bose-Einstein condensate (BEC) with an easy axis perpendicular to the plane, spins form magnetic domains that look similar to those of an Ising ferromagnet. Due to the superfluidity, domain growth exhibits  $R(t) \sim t^{2/3}$ , which is the same as the growth law for a binary fluid in the inertial regime, in the system [5]. If there is no superfluid flow in the ferromagnetic BEC, the spin dynamics is approximately the same as that of a ferromagnet and can be described by the Landau-Lifshitz-Gilbert (LLG) equation.

In this paper, we focus on the magnetic domain growth in a two-dimensional (2D) system, using the LLG equation. The LLG equation include a damping term, which is called the Gilbert damping. When the system has an easy-axis anisotropy, the Gilbert damping has the effect to direct spins to the easy-axis direction. Thus, if the easy axis is perpendicular to the  $x$ - $y$  plain, the system is an Ising-like ferromagnetic film, and the order parameter is the  $z$  component of spin. Without the damping, the order parameter is conserved. The damping term makes

the system non-conserved. The damping also causes energy dissipation. Energy dissipation seems essential for domain growth. However, domain growth is observed in some simulations without energy dissipation, i.e., without the damping term in the equation. Actually, the LLG equation without the Gilbert damping describes merely the precession of magnetization with a ferromagnetic interaction. We investigate what effects the damping have on coarsening dynamics and domain growth as well as what causes domain growth in the no-damping case.

The rest of the paper is organized as follows. In Sec. II, we describe the model and numerical procedures. Two characteristic length scales, which characterize domain size, are also introduced in this section. Numerical simulations are shown in Sec. III. The difference in domain growth between the cases with and without damping is demonstrated. In Sec. IV, we discuss why domain formation and domain growth occur even in the no-damping case. Finally, conclusions are given in Sec. V.

## II. MODEL AND METHOD

The model we use in numerical simulations is the LLG equation, which is widely used to describe the spin dynamics in ferromagnets. The dimensionless normalized form of the LLG equation is written as

$$\frac{\partial \mathbf{m}}{\partial t} = -\mathbf{m} \times \mathbf{h}_{\text{eff}} + \alpha \mathbf{m} \times \frac{\partial \mathbf{m}}{\partial t}, \quad (2)$$

where  $\mathbf{m}$  is the unit vector of spin,  $\alpha$  is the dimensionless Gilbert damping parameter. We here consider the 2D system lying in the  $x$ - $y$  plane, and assume that the system has a uniaxial anisotropy in the  $z$  direction and that no long-range interaction exists. Then, the dimensionless effective field is given by

$$\mathbf{h}_{\text{eff}} = \nabla^2 \mathbf{m} + C_{\text{ani}} m_z \hat{\mathbf{z}}, \quad (3)$$

where  $C_{\text{ani}}$  is the anisotropy parameter, and  $\hat{\mathbf{z}}$  is the unit vector in the  $z$  direction.

Equation (2) is mathematically equivalent to

$$\frac{\partial \mathbf{m}}{\partial t} = -\frac{1}{1+\alpha^2} \mathbf{m} \times \mathbf{h}_{\text{eff}} + \frac{\alpha}{1+\alpha^2} \mathbf{m} \times (\mathbf{m} \times \mathbf{h}_{\text{eff}}). \quad (4)$$

Solving Eq. (4), we perform numerical simulations. The initial condition is given as spins that are aligned in the  $x$  direction with a little random noises:  $m_x \simeq 1$  and  $m_y \simeq m_z \simeq 0$ . Simulations are performed in the  $512 \times 512$  lattice with periodic boundary conditions. Averages are taken over 50 independent runs.

The energy in this system is written as

$$E = \int d\mathbf{r} (\nabla \mathbf{m}(\mathbf{r}))^2 - C_{\text{ani}} \int d\mathbf{r} m_z(\mathbf{r})^2. \quad (5)$$

The first and second terms are the contributions from the interfacial and anisotropy energies, respectively. When  $C_{\text{ani}} > 0$ , the  $z$  component becomes dominant since a large  $m_z^2$  lowers the energy. Thus, we consider the spacial average of  $m_z$  as the order parameter of this system. If  $\alpha = 0$ , the average  $m_z$ , i.e., the order parameter, is conserved. The damping parameter  $\alpha$  also expresses the rate of energy dissipation, and the energy is conserved when  $\alpha = 0$ . In other words, the system is conserved and non-conserved fields for  $\alpha = 0$  and  $\alpha \neq 0$  cases, respectively.

Characteristic length scales of a domain pattern can be given in several ways. We here define two quantities to monitor domain growth. The first one is the average domain size  $R_c$  that is evaluated from the correlation function  $G(\mathbf{r}) = \langle m_z(\mathbf{r}) m_z(0) \rangle$ , where  $\langle \cdots \rangle$  denotes a spatial average. The Fourier transformation of  $G(\mathbf{r})$  is the structure factor

$$S(\mathbf{k}) = \langle \tilde{m}_z(\mathbf{k}) \tilde{m}_z(-\mathbf{k}) \rangle, \quad (6)$$

where  $\tilde{m}_z(\mathbf{k})$  is the Fourier transformation of  $m_z(\mathbf{r})$ . The average domain size  $R_c$  is defined by the distance where  $G(r)$  first drops to zero, and thus,  $G(R_c) = 0$ . The second one is the inverse of domain wall density,

$$R_d = \left[ 1 - \frac{1}{L_s^2} \int d\mathbf{r} m_z(\mathbf{r})^2 \right]^{-1}, \quad (7)$$

where  $L_s^2$  is the system size. It corresponds to the inverse perimeter density in the case of the Ising model [6–8].

### III. RESULTS

Domain patterns appear, regardless of the damping parameter  $\alpha$ . The snapshots in the upper row of Fig. 1 demonstrate that domain patterns at early times have no noticeable difference among the damping ( $\alpha = 0.03$ ) and no-damping ( $\alpha = 0$ ) cases. At later times, as shown in the bottom row of Fig. 1, remarkable difference appears especially around domain walls, although the average domain size looks almost the same. Domain walls, where

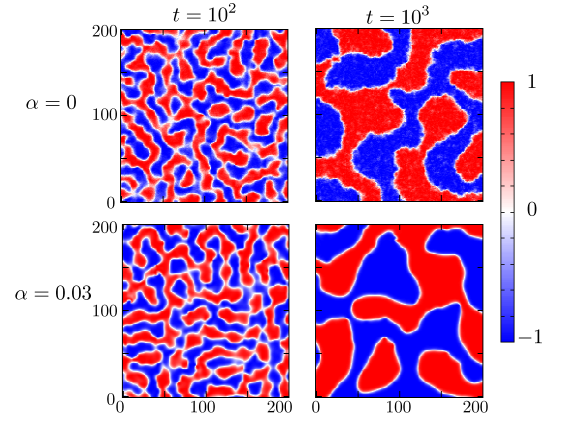


FIG. 1. (Color online) Snapshots of  $z$ -component  $m_z$  for  $\alpha = 0$  and  $0.03$  at time  $t = 10^2$  and  $10^3$ .

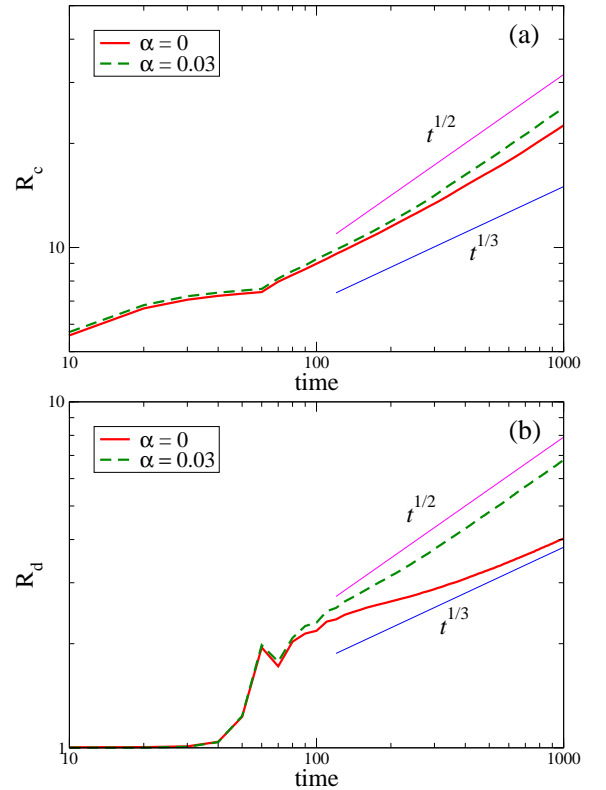


FIG. 2. (Color online) Time dependence of (a) the average domain size  $R_c$  and (b) the inverse of domain wall density  $R_d$ .

$m_z \simeq 0$ , are smooth in the damping case. However, in the no-damping case, they are rough. Moreover, in the snapshot of  $\alpha = 0$  at  $t = 10^4$ , small fractions of white ( $m_z = 0$ ) area are embedded in red ( $m_z = 1$ ) and blue ( $m_z = -1$ ) areas.

The characteristic length is expected to show a power-law growth at late times. However, growth laws seem to depend on the definition of the characteristic length of domain pattern. In Fig. 2, the time dependences of

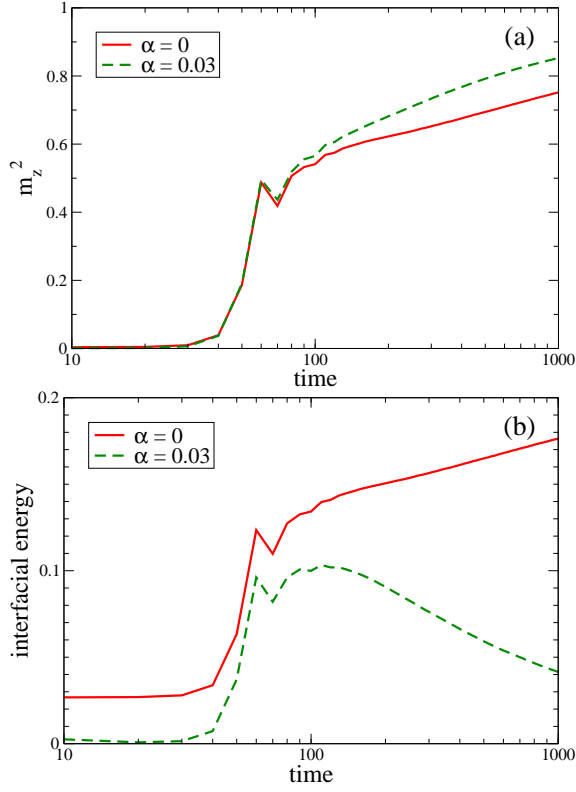


FIG. 3. (Color online) Time dependence of (a) the spatial average of  $m_z^2$  and (b) the interfacial energy.

the average domain size  $R_c$  and the inverse of domain wall density  $R_d$  are plotted for the dissipative and non-dissipative cases. The growth exponent is expected to be  $n = 1/3$  for  $\alpha = 0$  and  $n = 1/2$  for  $\alpha = 0.03$ . However, in Fig. 2 (a), growth exponents gradually changes, and no significant difference appears. The average domain size  $R_c$  does not reflect the details of domain structure but large-scale characteristics of domain pattern. This is related with the fact that we can hardly see a significant difference in the snapshots in each row of Fig. 1 at a glance. In contrast, in Fig. 2 (b), growth exponents approach to each of the expected values at late times. The domain wall density reflects the characteristics of small-scale structure as well as the large-scale characteristics. Thus,  $R_d$  is a better length scale than  $R_c$  to examine domain growth laws.

The difference in domain structure is closely connected with energy dissipation, which is shown in Fig. 3. Figure 3 (a) is directly related to Fig. 2 (b) through Eq. (7). The spatial average of  $m_z^2$  grows with time for both  $\alpha = 0$  and  $\alpha = 0.03$ . The interfacial energy, which is the first term of Eq. (5), decays after some time for  $\alpha = 0.03$  but increases for  $\alpha = 0$  in Fig. 3 (b). In other words, the energy dissipation that comes from the decline of the interfacial energy mainly causes the difference between the damping and no-damping cases. Smoothing domain-wall structure also contributes to the reduction of the

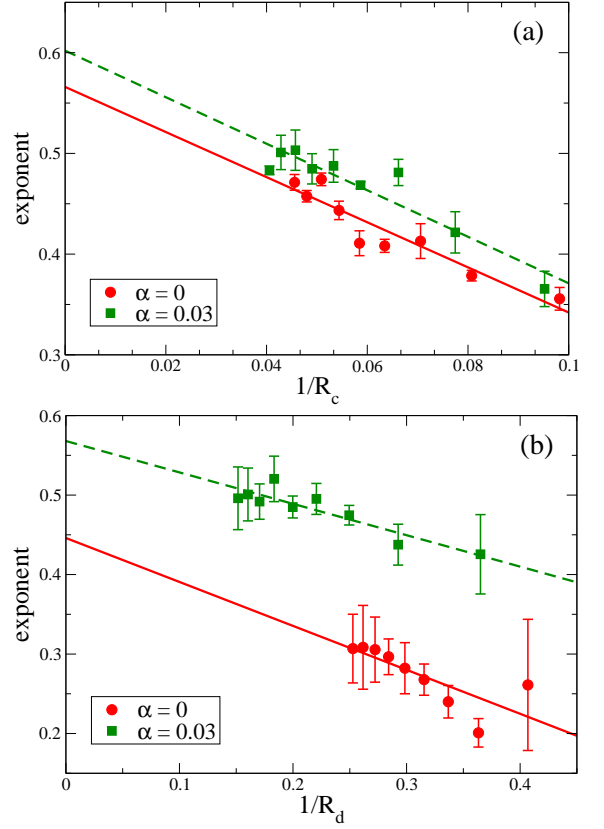


FIG. 4. (Color online) Effective exponents  $n_{\text{eff}}$  as functions of (a)  $1/R_c$  and (b)  $1/R_d$ . The solid and dashed lines are the fittings to Eq. (8) for  $\alpha = 0$  and  $0.03$ , respectively.

interfacial energy in the damping case. However, in the no-damping case, the interfacial energy increases with time to conserve the energy that is given by Eq. (5). In other words, the interfacial energy increases while the domain wall density decreases. This implies that the domain structure become more complex with time in the no-damping case.

The domain growth at late times in Fig. 2 shows power-law behavior, although exponents depend on time. The effective exponent, which is given by

$$n_{\text{eff}}(t) = \frac{d[\ln R(t)]}{d[\ln t]}, \quad (8)$$

is plotted as a function of  $1/R(t)$  in Fig. 4. The characteristic length  $R(t)$  is  $R_c$  and  $R_d$  in Figs. 4(a) and 4(b), respectively. According to Huse's formula [4], which was proposed to extract the asymptotic value of the growth exponent  $n$ , the finite-time effective exponent is approximately given by

$$n_{\text{eff}}(t) = n - \frac{a}{R(t)} + \dots, \quad (9)$$

where  $a$  is a constant [8]. The validity of the formula has been demonstrated by a lot of numerical works in conserved-field models [8–12].

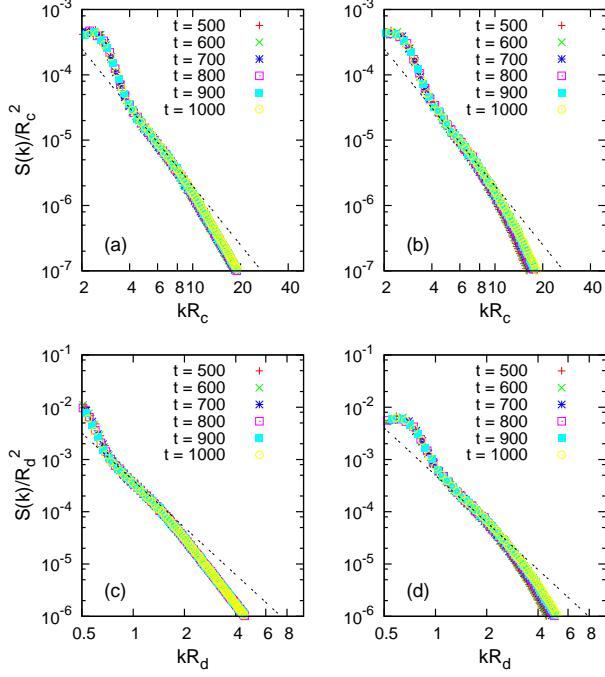


FIG. 5. (Color online) Scaling plots of the structure factor scaled with  $R_c$  for (a) and (b) and with  $R_d$  for (c) and (d).  $\alpha = 0$  for (a) and (c), and  $\alpha = 0.03$  for (b) and (d). The dashed lines indicate  $(kR)^{-3}$

Fitting the numerical data in Fig. 4(a) to Eq. (9), we obtain  $n \simeq 0.566 \pm 0.020$  ( $a = 2.24$ ) and  $n \simeq 0.602 \pm 0.021$  ( $a = 2.31$ ) for  $\alpha = 0$  and  $0.03$ , respectively. In both cases, the asymptotic value of  $n$  is estimated to be over  $1/2$ . This does not agree with conventional growth laws, and it is consistent with the result of Fig. 2(a). In Fig. 4(b), the fitting curves indicate  $n \simeq 0.446 \pm 0.053$  ( $a = 0.553$ ) and  $n \simeq 0.568 \pm 0.016$  ( $a = 0.395$ ) for  $\alpha = 0$  and  $0.03$ , respectively. However, the numerical data appear to be saturated at the expected value of each case, namely,  $n = 1/3$  for  $\alpha = 0$  and  $n = 1/2$  for  $\alpha = 0.03$ . This behavior is consistent with the result of Fig. 2(b).

Scaling behavior of coarsening dynamics also appears in structure factor. According to the Porod law, the structure factor has a power-law tail,

$$S(\mathbf{k}, t) \sim \frac{1}{R(t)k^{d+1}}, \quad (10)$$

where  $d$  is the dimension of the system [1]. Since  $d = 2$  in our system, Eq. (10) leads to  $S(\mathbf{k}, t)/R(t)^2 \sim [kR(t)]^{-3}$ . In Fig. 5,  $S(\mathbf{k}, t)/R(t)^2$  is plotted as a function of  $kR(t)$ . If the scaling length  $R(t)$  is chosen appropriately, the data at different times should be collapsed to one curve. Actually, partial collapse occurs in each plot. Although the data exhibit the expected behavior  $\sim k^{-3}$  in the middle- $k$  region, large- $k$  tails have steeper slopes than expected. The partial collapse of data and steeper slopes imply that the coarsening dynamics in this system is not exactly the

same as that of a conventional scalar field.

#### IV. DISCUSSION

We here have a naive question: Why does domain pattern formation occur even in the no-damping case? When  $\alpha = 0$ , Eq. (2) is just the equation of the precession of spin. Without damping, the formation of domains with large  $z$ -components seems to be counterintuitive. We here discuss how domain patterns are formed by means of the LLG equation.

Using the stereographic projection of the unit sphere of spin onto a complex plane [13], we rewrite Eq. (4) as

$$\frac{\partial \omega}{\partial t} = \frac{-i + \alpha}{1 + \alpha^2} \left[ \nabla^2 \omega - \frac{2\omega^*(\nabla \omega)^2}{1 + \omega\omega^*} - \frac{C_{\text{ani}}\omega(1 - \omega\omega^*)}{1 + \omega\omega^*} \right], \quad (11)$$

where  $\omega$  is a complex variable defined by

$$\omega = \frac{m_x + im_y}{1 + m_z}. \quad (12)$$

The fixed points of Eq. (11) are  $|\omega|^2 = 1$  and  $\omega = 0$ . The linear stability analysis about these fixed points tells us if domains can be formed.

At the fixed point  $\omega = 1$ ,  $m_x = 1$  and  $m_y = m_z = 0$ , which corresponds to the initial condition of the numerical simulation. Substituting  $\omega = 1 + \delta\omega$  into Eq. (11), we obtain linearized equations of  $\delta\omega$  and  $\delta\omega^*$ . Performing Fourier expansions  $\delta\omega = \sum_{\mathbf{k}} \delta\tilde{\omega}_{\mathbf{k}} e^{i\mathbf{k}\cdot\mathbf{r}}$  and  $\delta\omega^* = \sum_{\mathbf{k}} \delta\tilde{\omega}_{-\mathbf{k}}^* e^{i\mathbf{k}\cdot\mathbf{r}}$ , we have

$$\frac{d}{dt} \begin{pmatrix} \delta\tilde{\omega}_{\mathbf{k}} \\ \delta\tilde{\omega}_{-\mathbf{k}}^* \end{pmatrix} = \begin{pmatrix} \tilde{\alpha}_1(C_{\text{ani}} - k^2) & \tilde{\alpha}_1 C_{\text{ani}} \\ \tilde{\alpha}_2 C_{\text{ani}} & \tilde{\alpha}_2(C_{\text{ani}} - k^2) \end{pmatrix} \begin{pmatrix} \delta\tilde{\omega}_{\mathbf{k}} \\ \delta\tilde{\omega}_{-\mathbf{k}}^* \end{pmatrix}, \quad (13)$$

where  $\tilde{\alpha}_1 = \frac{1}{2}(-i + \alpha)/(1 + \alpha^2)$ ,  $\tilde{\alpha}_2 = \frac{1}{2}(i + \alpha)/(1 + \alpha^2)$ ,  $\mathbf{k} = (k_x, k_y)$ , and  $k = |\mathbf{k}|$ . The eigenvalues of the  $2 \times 2$  matrix of Eq. (13) are

$$\lambda(k) = \frac{\alpha}{2(1 + \alpha^2)}(C_{\text{ani}} - 2k^2) \pm \frac{\sqrt{4k^2(C_{\text{ani}} - k^2) + \alpha^2 C_{\text{ani}}^2}}{2(1 + \alpha^2)}. \quad (14)$$

Even when  $\alpha = 0$ ,  $\lambda(k)$  has a positive real part for  $k < \sqrt{C_{\text{ani}}}$ . Thus, the uniform pattern with  $m_x = 1$  is unstable, and inhomogeneous patterns can appear.

When  $\omega = 0$ ,  $m_x = m_y = 0$  and  $m_z = 1$ , which is also one of the fixed points. Substituting  $\omega = 0 + \delta\omega$  into Eq. (11) and performing Fourier expansions, we have the linearized equation of  $\delta\tilde{\omega}_{\mathbf{k}}$ ,

$$\frac{d}{dt} \delta\tilde{\omega}_{\mathbf{k}} = \frac{i - \alpha}{1 + \alpha^2}(k^2 + C_{\text{ani}})\delta\tilde{\omega}_{\mathbf{k}}. \quad (15)$$

This implies that the fixed point is stable for  $\alpha > 0$  and neutrally stable for  $\alpha = 0$ . In other words, when  $\alpha = 0$ , the fixed point  $\omega = 0$  is neither unstable nor attracting.

The initial condition, which is given as spins aligned in one direction with some noises in the  $x$ - $y$  plane, is the key to observe domain pattern formation in the no-damping case. Since the initial condition is unstable, the  $z$ -component of spin grows. Because of the short-range interaction, which is included in the effective field as the Laplacian term of Eq. (3), neighboring spins tend to direct in the same direction. Once  $m_z$  becomes  $\pm 1$ , it can keep the value even when  $\alpha = 0$ . Actually, if spins have totally random directions, no large domains are formed in the no-damping case, although domains are formed in damping cases ( $\alpha > 0$ ) from such an initial state.

## V. CONCLUSIONS

We have investigated the coarsening dynamics and domain growth in two-dimensional vector fields with an easy-axis anisotropy, using the LLG equation. Domain patterns are similar to those of scalar fields. However, domain growth and small-scale structure are slightly different between scalar fields and our system. The damping ( $\alpha \neq 0$ ) and no-damping ( $\alpha = 0$ ) cases correspond to non-conserved and conserved scalar fields, respectively.

The growth laws are in good agreement with expected ones when the inverse of domain wall density is taken as the characteristic length of domain. However, the average domain size  $R_c$ , which is defined from the correlation function, is inappropriate to distinguish the characteristics of domain pattern in the damping and no-damping cases. Since the energy is conserved in the no-damping case, the energy loss caused by domain growth is compensated by the gain of interfacial energy. This contributes to small-scale domain structure, which is not reflected in  $R_c$ .

The domain formation in the no-damping case looks counterintuitive, since the LLG equation without damping is merely the equation of the precession of spin. Actually, the initial state is the key to observe domain pattern formation in the no-damping case. The state in which spins are directed to almost the same in-plane direction is unstable, and domains with large out-of-plane components can grow from such an initial state.

## ACKNOWLEDGMENTS

This work was supported by MEXT KAKENHI (No. 26103514, “Fluctuation & Structure”).

- 
- [1] A. Bray, *Adv. Phys.* **43**, 357 (1994)
  - [2] I. M. Lifshitz and V. V. Slyozov, *J. Phys. Chem. Solids* **19**, 35 (1961)
  - [3] T. Ohta, D. Jasnow, and K. Kawasaki, *Phys. Rev. Lett.* **49**, 1223 (1982)
  - [4] D. A. Huse, *Phys. Rev. B* **34**, 7845 (1986)
  - [5] K. Kudo and Y. Kawaguchi, *Phys. Rev. A* **88**, 013630 (2013)
  - [6] A. Sadiq and K. Binder, *J. Stat. Phys.* **35**, 517 (1984)
  - [7] C. Roland and M. Grant, *Phys. Rev. B* **39**, 11971 (1989)
  - [8] C. Jeppesen and O. G. Mouritsen, *Phys. Rev. B* **47**, 14724 (1993)
  - [9] C. Yeung, *Phys. Rev. B* **39**, 9652 (1989)
  - [10] J. G. Amar, F. E. Sullivan, and R. D. Mountain, *Phys. Rev. B* **37**, 196 (1988)
  - [11] E. T. Gawlinski, J. Vinals, and J. D. Gunton, *Phys. Rev. B* **39**, 7266 (1989)
  - [12] W. Schleier, G. Besold, and K. Heinz, *J. Stat. Phys.* **66**, 1101 (1992)
  - [13] M. Lakshmanan and K. Nakamura, *Phys. Rev. Lett.* **53**, 2497 (1984)